PASJ: Publ. Astron. Soc. Japan **62**, 9–18, 2010 February 25

Study of the Large-Scale Temperature Structure of the Perseus Cluster with Suzaku

Sho NISHINO, Yasushi FUKAZAWA, and Katsuhiro HAYASHI
Department of Physical Science, Hiroshima University, 1-3-1 Kagamiyama, Higashi-Hiroshima, Hiroshima 739-8526
nishino@hep01.hepl.hiroshima-u.ac.jp
Kazuhiro NAKAZAWA
Department of Physics, The University of Tokyo, 7-3-1 Hongo, Bunkyo, Tokyo 113-0033
and
Takaaki TANAKA
Kavli Institute for Particle Astrophysics and Cosmology, Stanford University,
2575 Sand Hill Road M/S 29, Menlo Park, CA 94025, USA

(Received 2009 August 17; accepted 2009 November 5)

Abstract

We report on a study of the large-scale temperature structure of the Perseus cluster with Suzaku, using observational data of four pointings of the 30′ offset regions, together with data from the central region. Thanks to the Hard X-ray Detector (HXD-PIN: 10–60 keV), Suzaku can determine the temperature of hot galaxy clusters. We performed a spectral analysis by considering the temperature structure and the collimator response of the PIN correctly. As a result, we found that the upper limit of the temperature in the outer region is ~ 14 keV, and an extremely hot gas, which was reported for RX J1347.5−1145 and Abell 3667, was not found in the Perseus cluster. This indicates that the Perseus cluster has not recently experienced a major merger.

Key words: galaxies: clusters: individual (Perseus cluster) — X-rays: galaxies: clusters — X-rays: individual (Perseus cluster) — X-rays: spectra

1. Introduction

Clusters of galaxies are widely believed to grow up with the repetition of small-scale cluster merging. Gravitational energy released in the merger process heats up intracluster plasma, and accelerates particles up to higher energy. Actually, in many clusters, diffuse synchrotron radiation from high-energy electrons is detected by radio observations (e.g., A 2163: Feretti et al. 2001). In addition, a sign of hard X-ray emission, which is thought to be inverse Compton scattering of the Cosmic Microwave Background by accelerated electrons, has been reported for some clusters (e.g., Coma cluster: Fusco-Femiano et al. 1999). Moreover, large temperature fluctuations are often found in clusters that are candidates of non-thermal hard X-ray emitters. Recent X-ray studies have reported that very hot plasma, whose temperature exceeds ~ 20 keV, exists in some merging clusters, such as RX J1347.5−1145 (Ota et al. 2008) and A 3667 (Nakazawa et al. 2009). As stated above, plasma heating and particle acceleration in clusters are inseparably connected phenomena. Therefore, a search for these phenomena is important for understanding the history of cluster evolution, especially for the physical mechanisms of plasma heating and energy transportation.

In this paper, we report on a study of the large-scale temperature structure of the Perseus cluster (Abell 426). It is a nearby ($z = 0.0183$), massive, largely extended cluster, and is the most luminous cluster in the X-ray band. An X-ray bright active galaxy, NGC 1275, with a radio mini-halo, is located at the cluster center, and non-thermal power-law emission from NGC 1275 was confirmed by past observations (e.g., Sanders et al. 2005). ASCA found a large fluctuation of temperature in this cluster, and indicated that a very hot region with the temperature exceeding ~ 10 keV exists in the outer region. Information on cluster merging should remain in the low-density outer region rather than the dense central region. Therefore, it is very valuable to carefully investigate the temperature structure and non-thermal emission in the outer region of the cluster.

A determination of the temperature kT of hot regions with $kT \geq 10$ keV is difficult for detectors, whose energy bands are limited to below 10 keV (e.g., ASCA and XMM-Newton). Therefore, we should observe clusters with a detector that is sensitive above 10 keV, so as to determine the temperature by covering the spectral roll-off of thermal emission. Therefore, we observed 30′ offset regions from the Perseus cluster center, with the HXD-PIN/XIS (Takahashi et al. 2007; Kokubun et al. 2007; Koyama et al. 2007) aboard Suzaku (Mitsuda et al. 2007). HXD-PIN is a non-imaging detector comprising 64 PIN diodes, covering the hard X-ray band of 10–60 keV, and able to perform observations with a low-background level and a small field of view (FOV) of $34' \times 34'$ (FWHM). A narrow field of view has the advantage of reducing the contribution of the bright central region to the observed spectra. The XIS is equipped with four focal-plane CCD detectors with four co-aligned X-ray telescopes (XRT), covering the soft X-ray band of 0.2–10 keV with an FOV of $18' \times 18'$. The combination of the XIS and the HXD-PIN gives a broad-band X-ray spectrum, and we can thus determine the temperature structure of hot clusters. Throughout this paper, we adopt a Hubble constant

of $H_0 = 50h_{50}\,\mathrm{km\,s^{-1}\,Mpc^{-1}}$. All statistical errors are given at the 90% confidence level.

2. Observations and Data Reduction

We observed the outer regions of the Perseus cluster on 2006 September 2–4, with Suzaku. Four pointing observations of $30'$ offset regions from the cluster center were carried out. These observations made use of a narrow FOV of the PIN, by reducing the contribution of intense emission from the cluster center. Additionally, we also analyzed the Suzaku public data of observations of the Perseus cluster center, on 2006 February 1–2, August 29–September 2, and 2007 February 5–6. Figure 1 and table 1 summarize these observations.

We used version 2.0 pipeline processing data, and data screening was performed with HEAsoft version 6.2. HXD-PIN data were screened with a cut-off rigidity (COR) of > 6 GV, an elevation angle of $> 5°$ from the Earth rim, and good time intervals (GTI) during which the satellite was outside the South Atlantic Anomaly (SAA). We used ae_hxd_pinhxnome{1,2,3}_20080129.rsp for the HXD response matrix, and a "tuned" background (bgd-d) for the non X-ray background (NXB) (Fukazawa et al. 2009) of the PIN detector. Both were supplied by the HXD team (Fukazawa et al. 2009). The cosmic X-ray background (CXB) contribution for the HXD data was estimated by using the CXB parameters of Kirsch et al. (2005) and considering the collimator response, and then subtracted from the observed spectra as well as the NXB.

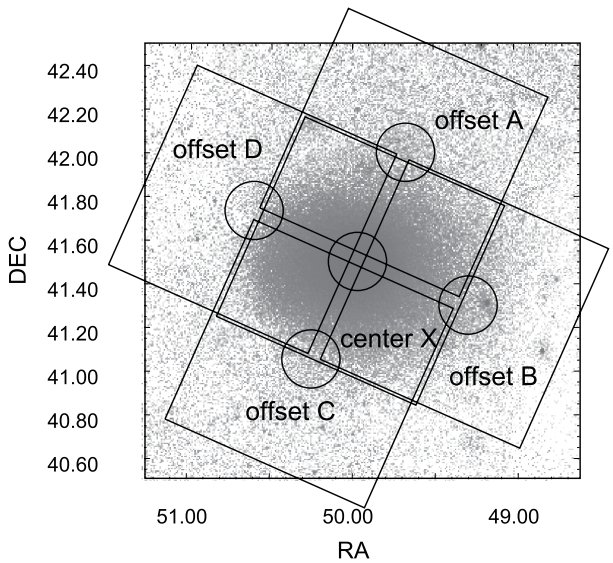

Fig. 1. 2° × 2° image of the Perseus cluster obtained with the ROSAT-PSPC (0.5–2 keV). The FOV of the center observation X and the offset observations A, B, C, D are shown on the image. Box shapes are the FOV of HXD-PIN (1° × 1°), and circles are the FOV of XIS ($8'$-radius).

Data screening of the XIS data was almost the same as that for the HXD, except for applying the criteria of COR > 8 GV and an elevation angle of $> 20°$ from the Earth rim. Response matrix files (rmf) and auxiliary response files (arf) were generated by the FTOOL xisrmfgen and xissimarfgen (Ishisaki et al. 2007), respectively, and the NXB was estimated by the FTOOL xisntebgdgen (Tawa et al. 2008).

3. Analysis and Results

Observed PIN spectra contain photons coming from a large sky area of the cluster, due to its FOV of $34' \times 34'$ (FWHM). Therefore, we have to take into account this effect to determine the temperature structure of the cluster. On the other hand, the XIS can obtain the spectrum of small regions, while it cannot determine the temperature of hot gas above 10 keV accurately, because of the limitations of the energy band below 10 keV. In the following analysis, we applied the APEC model to represent thermal emission from the intracluster plasma. Furthermore, we multiplied the plasma model by the WABS model, in order to take account of the photoelectric absorption in the Galactic intersteller medium. Projection effects in the line of sight are not considered here.

3.1. Nuclear Emission from NGC 1275

Nuclear X-ray emission from NGC 1275, which is located at the cluster center, has been reported by past studies, for example, XMM-Newton (Churazov et al. 2003), Chandra (Sanders et al. 2005) and Swift/BAT (Ajello et al. 2009). Therefore, we have to estimate the X-ray flux of the nucleus as contamination, to obtain an accurate temperature structure.

Figure 2 shows XIS images and radial surface brightness distributions in the 4–5 keV and 9–10 keV bands. The central excess is clearly confirmed in the XIS image within $1'$ radius, especially in the hard X-ray band. Taking into account the point-spread function of the XRT/XIS, this central excess is consistent with a point source, that is, nuclear emission of NGC 1275. We performed a spectral fitting for the

Table 1. Summary of Suzaku observations of the Perseus cluster for our analysis.

Position	Sequence No.	Date	RA/Dec (°)	Exposure (HXD/XIS)
Center X	800010010	2006/02/01–02	49.9504/41.5117	52 ks/41 ks
	101012010*	2006/08/29–09/02	49.9504/41.5117	129 ks/—
	101012020*	2007/02/05–06	49.9504/41.5117	41 ks/—
Offset A	801049010	2006/09/02–02	49.6833/42.0081	23 ks/23 ks
Offset B	801049020	2006/09/02–03	49.3167/41.3131	24 ks/24 ks
Offset C	801049030	2006/09/03–04	50.2625/41.0411	29 ks/29 ks
Offset D	801049040	2006/09/04–04	50.6125/41.7464	6 ks/6 ks

* Data of 101012010 and 101012020 were used only for the spectral analysis of the HXD-PIN.

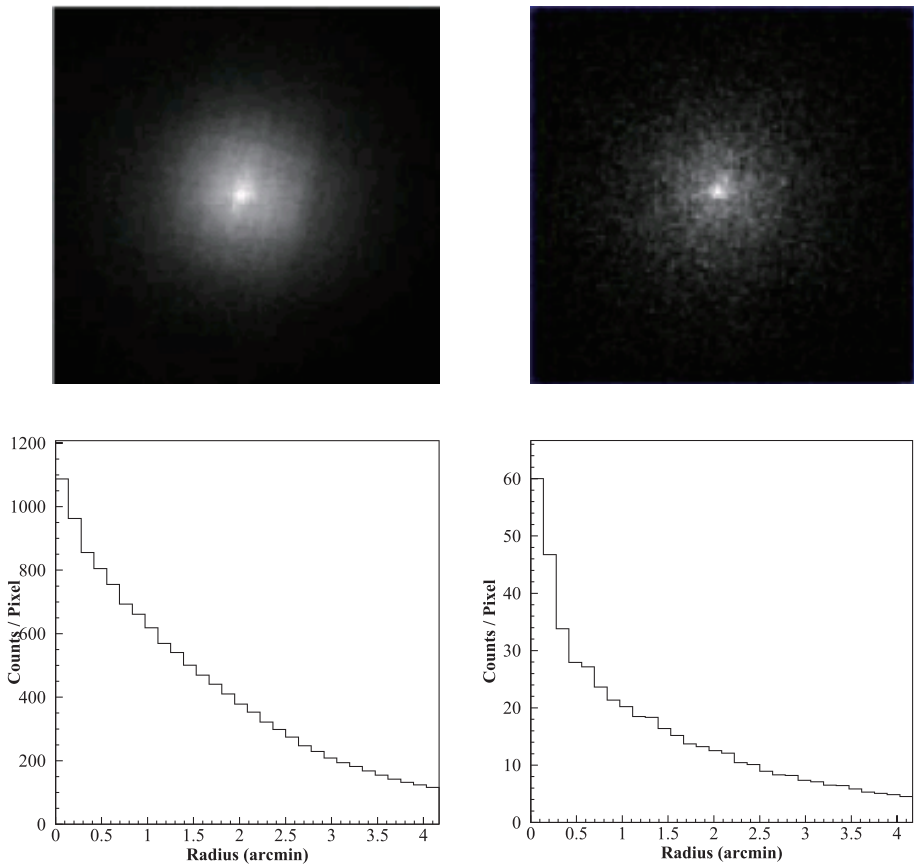

Fig. 2. Top panels are XIS images ($18' \times 18'$) extracted in the 4–5 keV (left) and 9–10 keV (right) bands. Bottom panels are radial surface brightness distributions extracted in the 4–5 keV (left) and 9–10 keV (right) bands.

region within $2'$ radius, with a single temperature APEC plus POWERLAW model. We generated the arf with xissimarfgen by using the XIS image within $2'$ from the cluster center as a seed image. Here, the photon index of the POWERLAW model is a free parameter. We show the spectrum and best-fit parameters in figure 3 and table 2, respectively. The fit improved from χ^2/d.o.f. $= 2.38$ to 1.31, when adding the POWERLAW model to the single-temperature APEC model. The estimated power-law luminosity is $\sim 5.6 \times 10^{43}$ erg s^{-1} (0.8–10 keV), in agreement with the value reported by Chandra (Sanders et al. 2005) of $\sim 6 \times 10^{43}$ erg s^{-1} (within $3'$ radius).

3.2. *Overall Properties*

In this section, as a preliminary step prior to the detailed analysis, we consider the overall properties of the cluster temperature structure. At first, we analyzed the XIS data of the cluster center to obtain the temperature structure in the central region. We divided the XIS events into 4 annular regions of $0'$–$2'$, $2'$–$4'$, $4'$–$6'$, $6'$–$8'$ in radius from the cluster center (figure 4). The result of $0'$–$2'$ is given in the previous subsection. For the regions of $2'$–$4'$, $4'$–$6'$, $6'$–$8'$, we performed a spectral fitting with a single-temperature APEC model. We generated the arf of each region with xissimarfgen by using the XIS image extracted in each spectral region as a seed image. Here, each region was assumed to be isothermal. Best-fit parameters for each region are summarized in table 3. The total flux of the 4 annular regions is approximately 1×10^{-9} erg cm^{-2} s^{-1} (0.8–10 keV), consistent with the past results of ASCA (Fukazawa et al. 2004). The obtained temperature decrement and abundance increment toward the center are roughly consistent with the past results of XMM-Newton (Churazov et al. 2003) and ASCA (Ezawa et al. 2001).

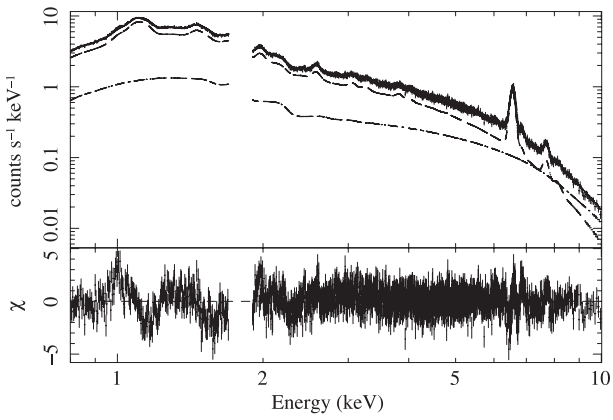

Fig. 3. XIS spectrum within $2'$ radius with the best-fit model WABS $\times$ (APEC + POWERLAW). Dashed lines in the upper panel show the APEC and POWERLAW contributions, respectively, and the residuals are shown in the bottom panel.

Table 2. Fitting results of the XIS spectrum within 2′ radius with the model WABS × (APEC + POWERLAW).

$N_{\rm H}$ ($\times 10^{21}\,{\rm cm}^{-2}$)	kT (keV)	Metal abundance (solar)	Photon index	Reduced χ^2 (χ^2/d.o.f.)	PL flux (0.8–10 keV) (erg cm^{-2} s^{-1})	Total flux (0.8–10 keV) (erg cm^{-2} s^{-1})
1.32 ± 0.01	3.25 ± 0.02	0.70 ± 0.01	1.61 ± 0.02	2048/1569	$(8.27 \pm 0.06) \times 10^{-11}$	$(2.92 \pm 0.01) \times 10^{-10}$

Table 3. Result of fits of XIS spectra in 2′–4′, 4′–6′, 6′–8′ annuli with the WABS × APEC model.

Region (radius)	$N_{\rm H}$ ($\times 10^{21}\,{\rm cm}^{-2}$)	kT (keV)	Metal abundance (solar)	Reduced χ^2 (χ^2/d.o.f.)	Flux (0.8–10 keV) (erg cm^{-2} s^{-1})
2′–4′	1.07 ± 0.01	4.60 ± 0.01	0.55 ± 0.01	3559/1696	$3.50 \pm 0.01 \times 10^{-10}$
4′–6′	1.05 ± 0.01	5.88 ± 0.05	0.47 ± 0.01	2018/1480	$2.33 \pm 0.01 \times 10^{-10}$
6′–8′	1.05 ± 0.01	6.45 ± 0.08	0.42 ± 0.01	1439/1158	$1.70 \pm 0.01 \times 10^{-10}$

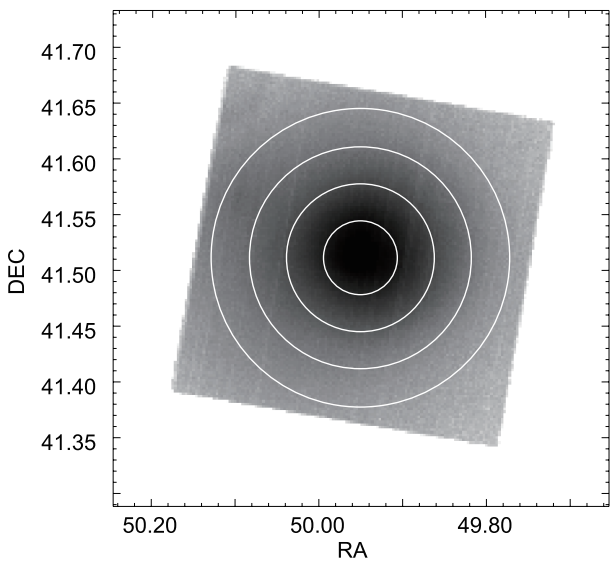

Fig. 4. XIS image of the center observation. The radii of the white circles are 2′, 4′, 6′, 8′ from the cluster center.

Next, we derived the temperature by using the PIN data of the central observation. The PIN data of the three center observations were added so as to obtain enough data statistics. The arf was generated by the FTOOL hxdarfgen. The current version of hxdarfgen calculates the arf for a point source. Therefore, for this analysis, we divided a 2° × 2° cluster image into 100 × 100 regions, and calculated the arf for each region. These arf files were weight-averaged by intensity, based on the cluster image of the ROSAT-PSPC.[1] We tried to fit the PIN spectrum with a single-temperature APEC model. Furthermore, in order to consider the emission from NGC 1275, we also tried to fit with a single-temperature APEC plus POWERLAW model. Here, the photon index of the power law was fixed to 1.61, which was obtained by an analysis of the XIS data in subsection 3.1. The metal abundance of 0.4 solar is an average value in the center region, obtained from the XIS spectral analysis. To avoid thermal noise of the PIN, we did not use any data below 15 keV for the spectral fitting. The fitting results are given in table 4 and figure 5. Without the POWERLAW model, the temperature is ∼7.2 keV. The estimated flux scaled to the total flux of the whole cluster region becomes 1.7×10^{-10} erg cm^{-2} s^{-1} (15–50 keV) or 1.8×10^{-9} erg cm^{-2} s^{-1} (0.8–10 keV), which is roughly consistent with the XIS results. With the POWERLAW, a temperature of ∼6.3 keV, and power-law luminosity of $\sim 2.5 \times 10^{43}$ erg s^{-1} were obtained.

Next, we tried to estimate the contribution of the central cool region to the PIN spectrum. We fitted the average XIS spectra within 8′ with a single-temperature APEC model, and obtained a temperature of 5.5 keV. Then, we fitted the PIN spectrum with a two-temperature APEC model plus power-law model. For one APEC model, the temperature and normalization were fixed to the values obtained from the above XIS analysis. Then, the temperature of the hot APEC component became $9.5^{+2.2}_{-1.7}$ keV. Therefore, the XIS and PIN spectra do not need an extremely hot component.

In the same way, we derived the temperature of each offset region, by using the offset XIS data (figure 6), with a single-temperature model. The absorption column density was fixed to 1.0×10^{21} cm^{-2}, which is the value obtained by the XIS analysis, as shown in table 3. Results are shown in table 5. The temperature is about 5–7 keV in any region, and a hot component with $kT > 10$ keV is not required for XIS spectra. If we adopt a higher absorption column density as 1.2 or 1.4×10^{21} cm^{-2}, a slightly lower, by less than ∼0.5 keV, temperature is required. The iron abundance is about 0.2–0.3 solar. These results are roughly consistent with those reported by ASCA (Ezawa et al. 2001).

We used the ROSAT-PSPC image of the Perseus cluster as a seed image of xissimarfgen, that is, the fluxes shown in table 5 were scaled to the total cluster flux, while taking account of the emission distribution of the cluster and the vignetting effect of the XRT. Then, the obtained flux of $\sim 1 \times 10^{-9}$ erg cm^{-2} s^{-1} (0.8–10 keV) is consistent with the XIS result of the center observation. This is also a consistency check that the XIS arf was correctly estimated.

For the PIN, the data were summed over four offset observations, because the emission from the offset regions is very faint for the PIN and sufficient statistics cannot be obtained

[1] SkyView ⟨http://skyview.gsfc.nasa.gov/⟩.

Table 4. Fitting results of the HXD-PIN spectrum of the cluster center observation with the model of APEC or APEC + POWERLAW.

kT (keV)	Metal abundance (solar)	Photon index	Reduced χ^2 (χ^2/d.o.f.)	PL flux (15–50 keV) (erg cm^{-2} s^{-1})	Total flux (15–50 keV) (erg cm^{-2} s^{-1})
7.2 ± 0.2	0.4 fixed	—	54/39	—	$(1.71 \pm 0.03) \times 10^{-10}$
6.4 ± 0.5	0.4 fixed	1.61 fixed	42/38	$(3.2 \pm 1.3) \times 10^{-11}$	$(1.81 \pm 0.05) \times 10^{-10}$

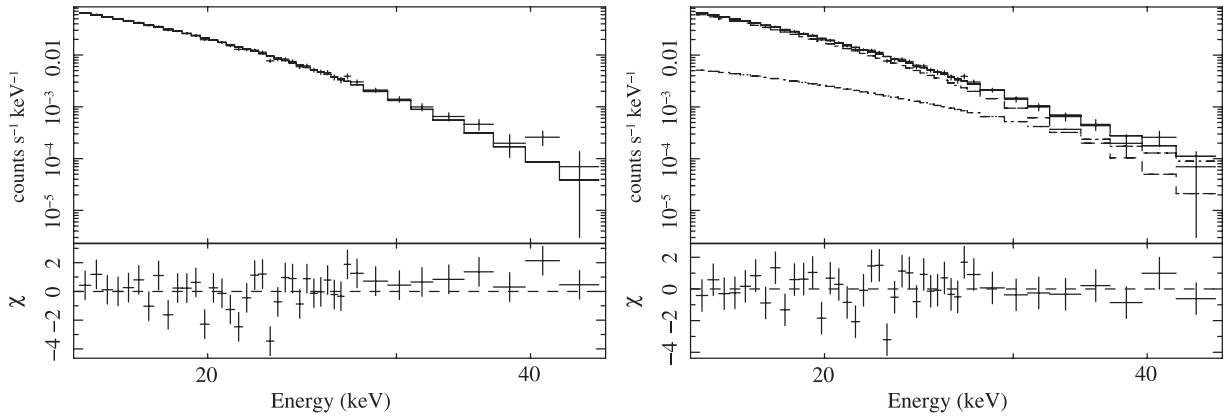

Fig. 5. Background-subtracted HXD-PIN spectrum of the center observation with the best-fit model of single-temperature APEC (left), and single-temperature APEC + POWERLAW (right). Dashed lines in the right upper panel are the same as in figure 3.

Table 5. Fitting results of XIS spectra of cluster offset observations with the model of WABS × APEC.

Region (area)	$N_{\rm H}$ ($\times 10^{21}$ cm^{-2})	kT (keV)	Metal abundance (solar)	Reduced χ^2 (χ^2/d.o.f.)	Flux (0.8–10 keV) (erg cm^{-2} s^{-1})
offset A	1.0 fixed	5.1 ± 0.2	0.28 ± 0.07	184/195	$(0.85 \pm 0.02) \times 10^{-9}$
offset B	1.0 fixed	5.3 ± 0.1	0.17 ± 0.03	435/440	$(1.47 \pm 0.01) \times 10^{-9}$
offset C	1.0 fixed	6.3 ± 0.2	0.21 ± 0.04	327/323	$(1.28 \pm 0.02) \times 10^{-9}$
offset D	1.0 fixed	5.8 ± 0.5	0.32 ± 0.15	46/50	$(1.03 \pm 0.04) \times 10^{-9}$

from the individual observation. We performed a spectral fitting by a single APEC model with the metal abundance fixed to 0.25 solar. The best-fit result is shown in figure 7 and table 6. The temperature was obtained to be 8 ± 2 keV, somewhat higher than the XIS results.

Next, we performed a joint-fit of the XIS spectrum and the PIN spectrum. Here, we summed over the four offset spectra of XIS. We fitted the spectra with a two-temperature APEC model. We fixed a lower temperature to 5.5 keV, which is the average temperature in the offset regions given in table 5. A higher temperature was set to be free. Then, a temperature of $8.7^{+3.3}_{-1.8}$ keV was obtained for the higher temperature. Therefore, the XIS and PIN spectra do not need an extremely hot component in the offset region.

3.3. Consideration of the PIN Collimator Response

In the previous section, we describe how we roughly obtained the averaged temperatures in the FOV, which are consistent with past observations. In this subsection, based on the above results, we investigate possible temperature structure by considering the collimator response of the PIN correctly. For that purpose, we implemented a Monte-Carlo simulator that reproduced the PIN spectra of the Perseus cluster by considering the assumed temperature structure and the collimator angular response of the PIN. By comparing simulated spectra with actual observed spectra, we could find the temperature structure that best reproduces the observed data. Here, we divided the cluster into six annular regions, 1–6, as shown in figure 8. The definition of region 1–4 is the same as in the previous XIS analysis of the center observation. As a first step, assuming the emission model parameters of region 1–4 to be those measured by XIS, we obtained the temperature of region 5 ($8' < r < 30'$) by using the PIN data of the center observation. Next, assuming the temperature of region 5 to be the value obtained in the first step, as well as the region 1–4 temperature, we obtained the temperature of region 6 ($30' < r < 60'$) by using PIN data of the offset observations.

At first, we prepared the emission-spectral model with an assumed temperature, for each region of region 1–6. The spectral model was created between 0.1–100 keV with 256 bins on a linear scale by the Xspec APEC model. In the simulator, we determined a random position of generated photons. We

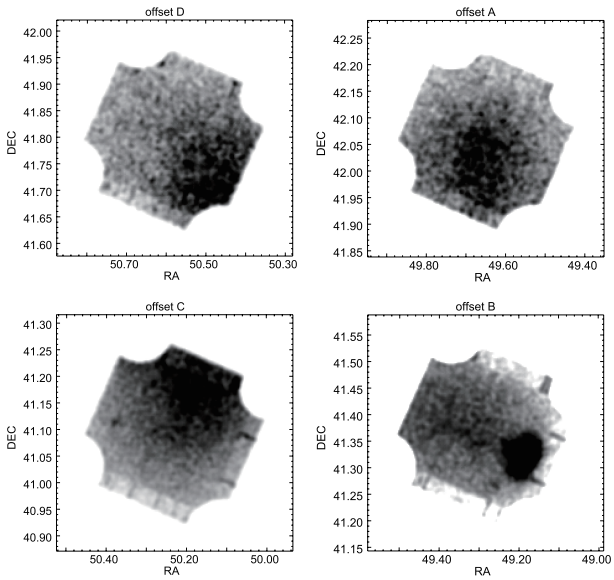

Fig. 6. XIS images of offset A, B, C, D observations. Calibration source regions at the corners of each image are subtracted. A point source, IC 310, is visible in the FOV of the offset B observation.

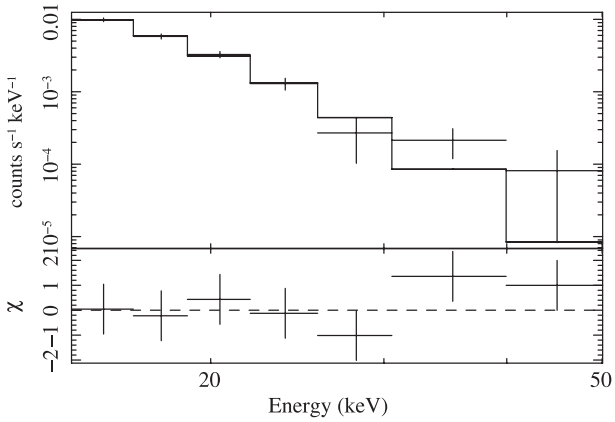

Fig. 7. Background-subtracted HXD-PIN spectrum of the offset observations with the best-fit single-temperature APEC model.

used a 2° × 2° ROSAT-PSPC image of the Perseus cluster (figure 9a) as a seed photon map. The image was divided into 40 × 40 regions whose size was 3′ × 3′. Then, we randomly determined the energy of generated photons, following the emission spectral model that we assumed above. Next, thus-generated photons were filtered by an angular response map, which was created by the FTOOL hxdarfgen for each observation. An example of the angular response map for 30 keV photons is shown in figure 9b. The transmission efficiency of the collimator was almost constant below an energy of 50 keV. The number of simulated photons was 10^7 for each observation. The output was a spectrum to which only the angular response of the PIN detector was applied. The simulated spectrum was read into Xspec as a model, and compared with the observed spectrum by spectral fitting, after the rmf was applied to the model. Here, only the normalization of the model was a free parameter.

Table 6. Fitting results of the HXD-PIN spectrum of the cluster offset observations with the APEC model.

kT (keV)	Metal abundance (solar)	Reduced χ^2 (χ^2/d.o.f.)	Total flux (15–50 keV) (erg cm^{-2} s^{-1})
$7.82^{+2.05}_{-1.46}$	0.25 fixed	4.1/5	$1.25^{+0.08}_{-0.36} \times 10^{-10}$

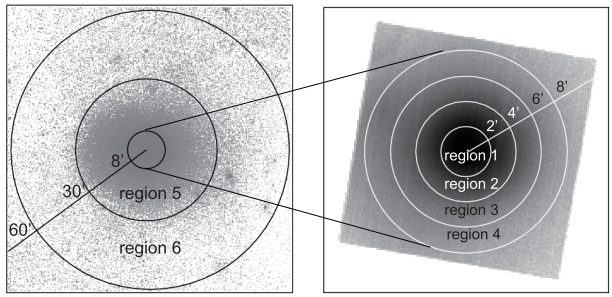

Fig. 8. Definition of six cluster regions. The radii of circles are 2′, 4′, 6′, 8′, 30′, 60′ from the cluster center.

First, we obtained the temperature of region 5, using the PIN data of the center observation. The emission models of region 1–4 were based on the XIS results in tables 2 and 3. The temperature of region 5 was tested from 5 keV to 12 keV with a step of 0.5 keV, with the metal abundance fixed to 0.35 solar. The emission model of region 6 was still unknown, and thus assumed to be the same as that of region 5. The fraction of incident photons from region 6 was approximately 1% of all photons, and thus their contribution was negligible. Moreover, the contamination of point sources in the FOV, for example IC 310 shown in the XIS image of the offset B observation, was less than 1% of all photons, and thus their contribution was also negligible. We compared each simulated spectrum with the observed spectrum by adjusting the model normalization. The χ^2 distribution for the temperature of region 5 is shown in figure 10 (left). Here, the uncertainties of the XIS model parameters in region 1–4 were taken into account, and error ranges are shown in the figure as dashed lines. The best-fit temperature of region 5 is 7 keV, and the error range is 6.6–7.4 keV at the 90% confidence level. Figure 10 (right) shows the best-fit model and spectrum. The fraction of the photon flux from region 1–6 in the best-fit simulated spectrum is 6.2%, 17.0%, 25.5%, 15.8%, 34.4%, 1.1%.

Next, to obtain the temperature of region 6 ($30' < r < 60'$), we adopted the temperature of 7 keV for region 5, which was as described above, in addition to the emission model of region 1–4. The temperature of region 6 was tested from 5 keV to 15 keV with a step of 1 keV, with the metal abundance fixed to 0.25 solar. We investigated the averaged-temperature of the four offset regions, by using the PIN spectrum summed over the four observations, as described in subsection 3.1, and compared it with the simulated spectrum. The results are shown in figure 11. The best-fit temperature of region 6 is ∼9.0 keV. The upper limit is ∼14 keV at the 90% confidence level, while the lower limit is not well constrained. The fraction of photon flux from region 1–6 in the best-fit simulated

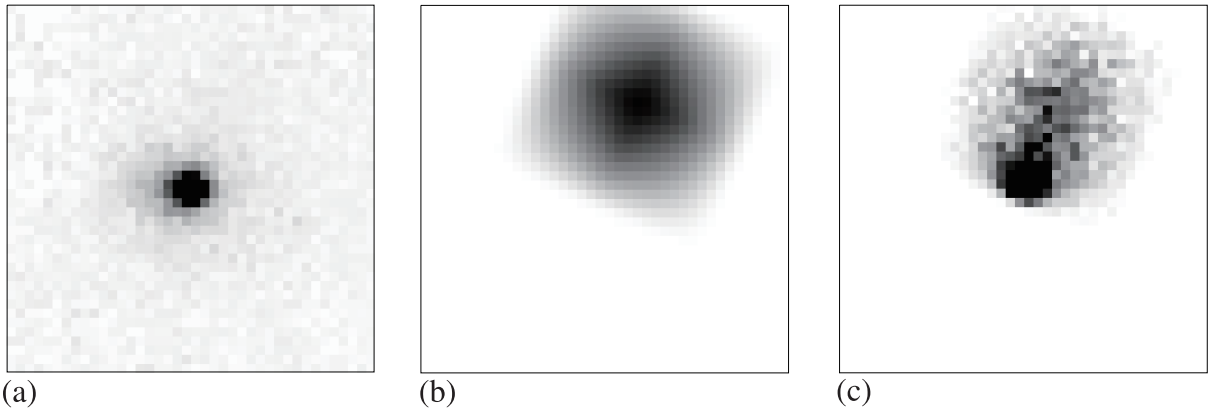

Fig. 9. (a) ROSAT-PSPC image of the Perseus cluster ($2^\circ \times 2^\circ$). (b) Angular response map for the offset A observation for 30 keV photons. (c) Probability map of incident direction of photons in the simulation, i.e., map (a) × map (b).

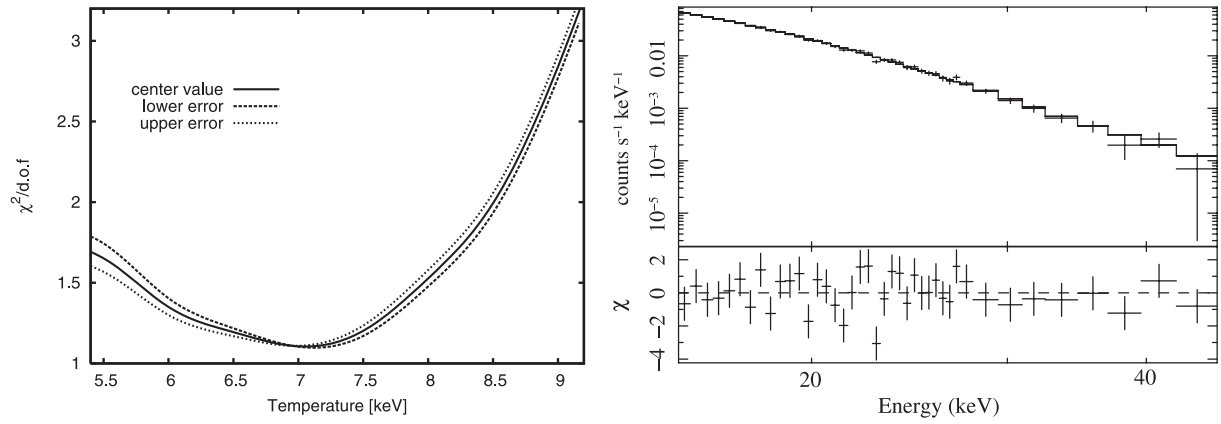

Fig. 10. (Left) Reduced χ^2 of the difference between the actual spectrum and simulated spectrum for region 5. (Right) Background-subtracted HXD-PIN spectrum of the center observation with the best-fit model (kT of region 5 is 7.0 keV).

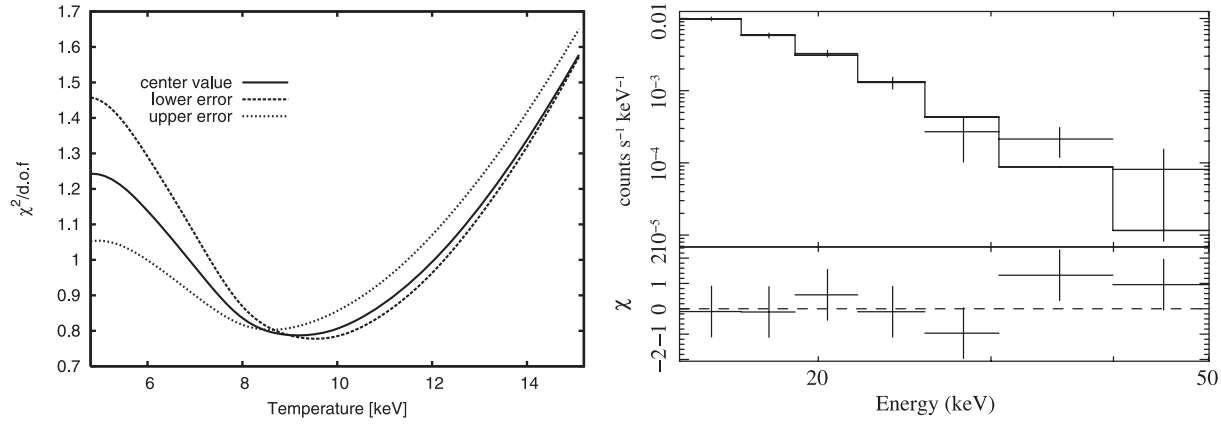

Fig. 11. (Left) Reduced χ^2 of the difference between the actual spectrum and simulated spectrum for region 6. (Right) Background-subtracted HXD-PIN spectrum of the offset observation with the best-fit model (kT of region 6 is 9.0 keV).

spectrum is 2.9%, 7.8%, 14.3%, 11.0%, 40.2%, 23.8%. The number of photons from regions 5 and 6 is more than 60%, and the contribution from the central region is not so large in the offset observation. In fact, the temperature in region 6 does not depend so much on the power-law flux of NGC 1275. We considered the systematic errors due to the uncertainty of the NXB of HXD-PIN. The HXD-team announces that NXB models released by them have a ±3% uncertainty (Fukazawa

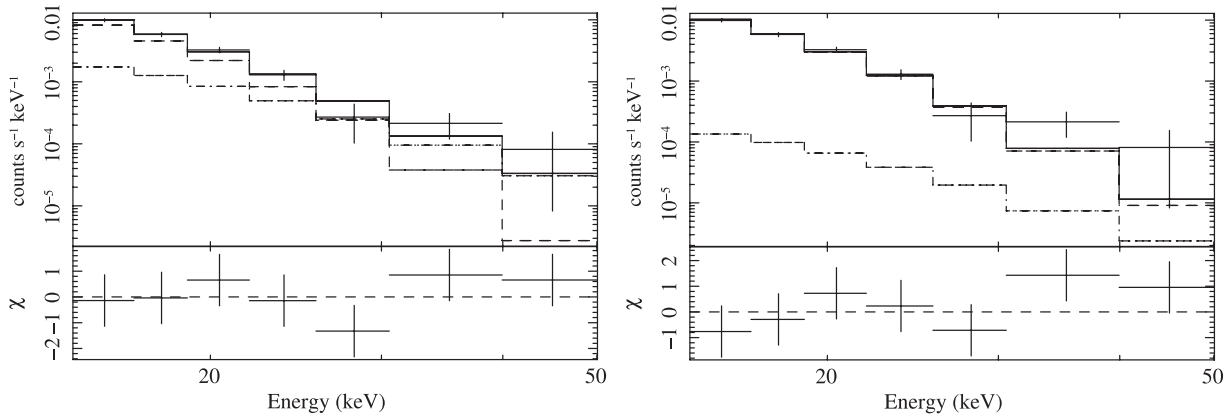

Fig. 12. Background-subtracted HXD-PIN spectra of the offset observations with the best-fit single temperature APEC plus POWERLAW model (left), with the best-fit simulated thermal model plus POWERLAW model (right). Dashed lines in the upper panels show the APEC (left)/simulated thermal (right) and POWERLAW contributions.

Table 7. Fitting results of the PIN spectra of the offset observations.

Photon index	Reduced χ^2 (χ^2/d.o.f.)	PL flux (15–50 keV) (erg cm^{-2} s^{-1})	Total flux (15–50 keV) (erg cm^{-2} s^{-1})
2.0 fixed	4.7/5	4.38×10^{-12} (upper limit)	1.22×10^{-10}

et al. 2009). When we decreased the NXB by 3%, the upper limit of the temperature became 7.9 keV for region 5 and 19 keV for region 6.

3.4. Constraints to Non-Thermal Emission from the Cluster

Here, we constrain the non-thermal emission hidden by the thermal emission in the offset region of the Perseus cluster. First, we performed a naive spectral fitting for the offset PIN spectrum as in subsection 3.2 (without considering the PIN collimator response), with a model consisting of a single-temperature APEC plus POWERLAW. Here, the metal abundance was fixed to 0.25 solar and the photon index of the POWERLAW model was fixed to 2.0. The best-fit spectrum is shown in figure 12 (left). A POWERLAW component with a flux of 5.6×10^{-11} erg cm^{-2} s^{-1} (15–50 keV) was marginally required, but the significance is low.

Next, we performed a spectral fitting by considering the PIN collimator response as described in subsection 3.3. We applied a simulated model where the temperature of region 6 was assumed to be 7 keV, the same as for region 5. In this case, a more realistic upper limit was obtained than the naive analysis because the temperature gradient at the center region and the hard emission from NGC 1275 were taken into account in this analysis. Actually, a tighter upper limit of 4.4×10^{-12} erg cm^{-2} s^{-1} was obtained, as shown in figure 12 (right) and table 7 (bottom).

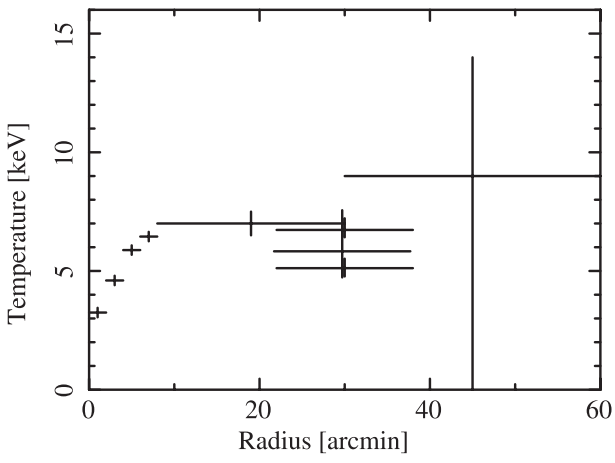

Fig. 13. Radial temperature profile of the Perseus cluster, obtained in this work. The first four crosses from the center are obtained with the XIS in subsection 3.1 and subsection 3.2, crosses around 20′ and 45′ are obtained with the PIN in subsection 3.3. Furthermore, temperatures obtained from XIS offset observations are shown at 30′ for the offset C, D, A in order of temperature decreasing. The temperature of offset B containing emission from IC 310 is not shown here. Error bars in the figure present 90% confidence level.

4. Discussion

4.1. Temperature Structure

The radial temperature profile obtained in this work is shown in figure 13. Error bars in the figure present the 90% confidence level, though systematic errors due to the NXB uncertainty of the HXD-PIN are not shown here. Distinct features of the temperature structure are a steep decline toward the center and a relatively flat profile in the outer region. XIS results in the offset regions give a lower temperature than the PIN analysis. This is possibly because the XIS is sensitive to a lower temperature component, if two different temperature (hot and cool) components exist at different regions along the same line of sight. Therefore, the results of the XIS and the PIN do not necessarily conflict with each other. Most importantly,

we found that the upper limit of the temperature of the offset region, where hot components seem to exist, is at most 14 keV (< 19 keV within the systematic errors). Considering that the XIS spectra do not require the hot component, it seems that very hot gas, as reported in RX J1347.5−1145 (Ota et al. 2008) or A 3667 (Nakazawa et al. 2009), does not exist in the Perseus cluster. In this analysis, we could not study temperature fluctuations due to the low data statistics of the offset observations. But the average temperature of the four offset regions is not inconsistent with the results of ASCA (Furusho et al. 2001).

The temperature structure with a negative gradient towards the center and a roughly flat external plateau is typical for cooling flow-type clusters (Pointecouteau et al. 2005). These clusters, showing a strong cooling core, are thought to be gravitationally relaxed. Actually, most colliding-type clusters do not show such a cooling core. Therefore, we infer that the main body of the Perseus cluster had already been relaxed, and had not recently experienced a violent cluster merger, which greatly influences the temperature structure of the cluster. On the other hand, ROSAT and other X-ray observatories found an excess of the surface brightness at $20'$ east from the cluster center (Ettori et al. 1998). Moreover, ASCA found a temperature drop at the corresponding region (Furusho et al. 2001). Therefore, it is implied that a small-scale substructure, such as a small galaxy cluster or group with cool gas, is currently colliding with the main body of the Perseus cluster.

We consider two reasons why extremely hot gas does not exist in the Perseus cluster, even though some evidence of the cluster merger was found as described above. The first reason is that the present merging is in the latest phase, that is, extremely hot gas heated in the long past has already cooled down. The second reason is that the heating condition is not satisfied in the current merging. In the case of RX J1347.5−1145 (Ota et al. 2008), though it depends on various cluster parameters, extremely hot gas seems to take approximately 0.5×10^9 yr to cool down by radiation. On the other hand, the cold substructure in the Perseus cluster must have been created in recent 10^9 yr, considering the diffusion time of the intracluster medium (ICM) (Furusho et al. 2001), and this is roughly comparable to the cooling time of extremely hot gas. Accordingly, the picture that only the extremely hot gas cooled down without diffusion of the cold gas is not natural. Therefore, the first reason, that a violent cluster merger occurred in the long past and extremely hot gas has already cooled down, is unlikely. Hence, the second reason is preferred. According to Kitayama et al. (2004) and Ota et al. (2008) with the help of Takizawa (1999), a high-velocity ($\Delta v \sim 4500\,\mathrm{km\,s^{-1}}$) collision of two massive ($5 \times 10^{14}\,M_\odot$) clusters is needed to heat the ICM up to 20 keV or higher for RX J1347.5−1145. In the case of the Perseus cluster, the total mass, including the cold substructure, is $1.2 \times 10^{15} M_\odot$, according to Ettori, Fabian, and White (1998). However, the mass of the subcluster is much less than the total mass, probably by one or two orders of magnitude. Then, it may be difficult to heat up the ICM to a high temperature, if the mass difference of two merging clusters is very large. Actually, according to Takizawa (1999), two-cluster merging, with a mass ratio of 4, could heat up the ICM to at most ~ 13 keV. Therefore, it is inferred that the current Perseus cluster has already grown up enough, and is not in a violent merger phase. Though this is just speculation, the history of the cluster formation may be divided into two phases. In the early phase, clusters or groups with almost the same mass repeat violent mergers and grow up. In the latest phase, a grown-up large cluster cannibalizes small-scale galaxies clusters or groups. Therefore, a comparison between the spatial distribution of merging clusters and relaxed clusters is interesting to understand the evolution of the galaxy clusters and the large-scale structure of the universe.

4.2. Non-Thermal Emission from the Perseus Cluster

In our analysis, we obtained the upper-limit flux of the non-thermal emission as $4.4 \times 10^{-12}\,\mathrm{erg\,cm^{-2}\,s^{-1}}$ (15–50 keV) at the cluster offset region. So far, the Perseus cluster has often been observed by X-ray satellites, such as ASCA, XMM-Newton, Chandra, Swift/BAT (Ajello et al. 2009) and so on. However the non-thermal emission from the cluster, itself, has not been discussed well, because the thermal emission from the cluster core is very bright and furthermore the AGN emission from NGC 1275 must be considered. In this paper, we performed observations of cluster offset regions, by reducing the bright emission from the cluster center. In addition, we considered the contribution of the AGN emission from NGC 1275. Therefore, this may be the first robust result of an upper limit of non-thermal emission from the Perseus cluster. Assuming the distance to the Perseus cluster to be 75 Mpc, the corresponding upper limit luminosity is $3.0 \times 10^{42}\,\mathrm{erg\,s^{-1}}$. This limit is tighter than those of other clusters observed with Suzaku HXD-PIN, such as A 3376 (Kawano et al. 2009) and A 3667 (Nakazawa et al. 2009), owing to the proximity of the Perseus cluster. Considering no report of radio detection of the synchrotron emission, there is yet no evidence of particle acceleration in the Perseus cluster. This result also supports that the Perseus cluster is not in a violent cluster merger phase, as inferred from the ICM temperature studies.

The authors thank Dr. Jelle Kaastra for careful reading and many useful comments. The authors also thank the Suzaku team for development of hardware/software and operation. SN is supported by Research Fellowships of the Japan Society for the Promotion of Science for Young Scientists.

References

Ajello, M., et al. 2009, ApJ, 690, 367
Churazov, E., Forman, W., Jones, C., & Böhringer, H. 2003, ApJ, 590, 225
Ettori, S., Fabian, A. C., & White, D. A. 1998, MNRAS, 300, 837
Ezawa, H., et al. 2001, PASJ, 53, 595
Feretti, L., Fusco-Femiano, R., Giovannini, G., & Govoni, F. 2001, A&A, 373, 106
Fukazawa, Y., et al. 2009, PASJ, 61, S17

Fukazawa, Y., Makishima, K., & Ohashi, T. 2004, PASJ, 56, 965
Furusho, T., Yamasaki, N. Y., Ohashi, T., Shibata, R., & Ezawa, H. 2001, ApJ, 561, L165
Fusco-Femiano, R., Dal Fiume, D., Feretti, L., Giovannini, G., Grandi, P., Matt, G., Molendi, S., & Santangelo, A. 1999, ApJ, 513, L21
Ishisaki, Y., et al. 2007, PASJ, 59, S113
Kawano, N., et al. 2009, PASJ, 61, S377
Kirsch, M. G. F., et al. 2005, Proc. SPIE, 5898, 22
Kitayama, T., Komatsu, E., Ota, N., Kuwabara, T., Suto, Y., Yoshikawa, K., Hattori, M., & Matsuo, H. 2004, PASJ, 56, 17
Kokubun, M., et al. 2007, PASJ, 59, S53
Koyama, K., et al. 2007, PASJ, 59, S23
Mitsuda, K., et al. 2007, PASJ, 59, S1
Nakazawa, K., et al. 2009, PASJ, 61, 339
Ota, N., et al. 2008, A&A, 491, 363
Pointecouteau, E., Arnaud, M., & Pratt, G. W. 2005, A&A, 435, 1
Sanders, J. S., Fabian, A. C., & Dunn, R. J. H. 2005, MNRAS, 360, 133
Takahashi, T., et al. 2007, PASJ, 59, 35
Takizawa, M. 1999, ApJ, 520, 514
Tawa, N., et al. 2008, PASJ, 60, S11